

Resonance phenomena in a nanomagnet coupled to a Josephson junction under external periodic drive

K. V. Kulikov ^{1,2}, D. V. Anghel ^{1,3}, M. Nashaat ^{1,4}, M. Dolineanu^{3,5}, M. Sameh ^{1,4} and Yu. M. Shukrinov^{1,2,6}

¹*Bogolyubov Laboratory of Theoretical Physics, Joint Institute for Nuclear Research, Dubna, Moscow region 141980, Russia*

²*Dubna State University, Dubna, Moscow region 141980, Russia*

³*Horia Hulubei National Institute for R&D in Physics and Nuclear Engineering, Măgurele, Romania*

⁴*Department of Physics, Faculty of Science, Cairo University, 12613 Giza, Egypt*

⁵*University of Bucharest, Faculty of Physics, 077125 Măgurele, Romania*

⁶*Moscow Institute of Physics and Technology, Dolgoprudny 141700, Russia*



(Received 28 July 2023; revised 8 January 2024; accepted 8 January 2024; published 26 January 2024)

We investigate resonance phenomena in a system consisting of a nanomagnet coupled to a Josephson junction under external periodic drive. The coupling in the system leads to the appearance of additional resonance peaks whose properties depend on the periodic signal and Josephson junction dynamics. In the linear regime, we derive an analytical description of the resonance phenomena which are then confirmed by numerical simulations. This analytical method is universal and can also be applied to Josephson junctions with an anomalous phase shift in the current phase relation. This work provides a method for controlling the resonances of hybrid structures that might be interesting for applications.

DOI: [10.1103/PhysRevB.109.014429](https://doi.org/10.1103/PhysRevB.109.014429)

I. INTRODUCTION

One of the most interesting recent developments in magnetism is the ability to fabricate nanometer-scale magnets [1–8]. These nanomagnets possess magnetic properties which are different from those of bulk materials and can provide advanced replacements for hard disk media [9,10] and computer memory chips [11]. Recently, molecular nanomagnets have also been studied as potential candidates for qubit realization [12]. Such a realization is expected to play a crucial role in quantum information processing [13] and spintronics [14,15].

The dynamics of the magnetization of molecular nanomagnets can be described by the Landau-Lifshitz-Gilbert (LLG) equation [16,17]. It is well known that if a material is magnetized by an external magnetic field, the magnetization vector \mathbf{M} becomes parallel to the external magnetic field. When the external magnetic field frequency coincides with the eigenmode of the precession of magnetic moments of the electronic system of the ferromagnet, a ferromagnetic resonance (FMR) is achieved [16,18,19]. In this case, spin waves are excited in the ferromagnet and can be viewed as both spatial and time dependent variations in the magnetization [16,17]. Experimentally, FMR was observed by Griffiths [20], who found that FMR does not occur exactly at the resonance frequency $\Omega_r = \gamma H$, (where γ is the electron gyromagnetic ratio and H is the internal magnetizing field). Furthermore, Kittel proposed that the ferromagnetic resonance condition should be modified from the original Landau-Lifshitz theory by taking into account the shape and the crystalline anisotropy through the demagnetizing fields [21]. The FMR technique can provide information on the magnetization, magnetic anisotropy, dynamic exchange/dipolar energies, and relaxation times, as well as the damping in the magnetization dynamics [19]. In Ref. [22], dynamic fluctuations of nanoparticles and

their anisotropic behavior were recorded by the FMR signal. The FMR modes for $\text{Fe}_{70}\text{Co}_{30}$ magnetic nanodots in a monodomain state under different in-plane and out-of-plane magnetic fields were studied in Ref. [23]. The FMR technique can be applied to several systems, like monolayers [24], multilayers, ultrathin films [25–27], and nanosystems [28–31]. The direct coupling between the magnetic moment and Josephson oscillations realized in a Josephson junction (JJ) coupled to a ferromagnet manifests the unique properties of the ferromagnetic resonance such as the appearance of Shapiro-like steps in the IV-characteristics, different stable magnetic trajectories, Duffing oscillator features, etc., [16,32–35].

Recently, a dramatic increase in the FMR frequency in the presence of electronic interaction between superconducting and ferromagnetic layers, which was due to the coupling of the magnetization dynamics and superconducting imaginary conductance at S-F interfaces, was proposed theoretically in Ref. [36]. This was confirmed experimentally in Ref. [37], where the authors considered superconductor-ferromagnet-superconductor thin film structures and observed a broad-band ferromagnetic resonance for a large set of samples with varied thickness of both superconducting and ferromagnetic layers in wide frequency and temperature ranges.

A system formed of a nanomagnet coupled to a JJ was analyzed in [38]. The magnetic field of the nanomagnet influences the superconducting current in the JJ, and vice versa, the electromagnetic field created by the JJ acts upon the nanomagnet. Several features are predicted to appear as a result of this mutual interaction, like, for example, a spin flip produced by a specific time variation of the external voltage.

The superconducting current of a JJ coupled to an external nanomagnet driven by a time-dependent magnetic field both without and in the presence of an external ac drive was studied in Ref. [39]. The authors showed the existence of Shapiro-type

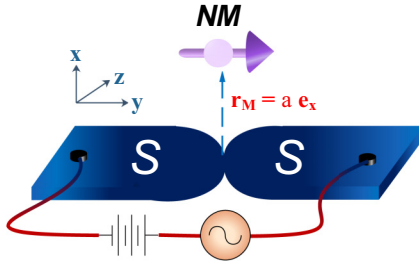


FIG. 1. Schematic diagram of the considered system with system geometry.

steps in the IV characteristics of the JJ subjected to a voltage bias for a constant or periodically varying magnetic field and explored the effect of rotation of the magnetic field and the presence of an external ac drive on these steps [39]. Furthermore, a uniform precession mode (spin wave) could be excited by a microwave magnetic field, at ferromagnetic resonance (FMR), when all the elementary spins precess perfectly in phase [40].

An analogy between the Kapitza pendulum and the JJ-nanomagnet system was introduced in Ref. [41], and it was shown that the magnetic moment of the nanomagnet can be reoriented. In this case, the Josephson to magnetic energy ratio G corresponds to the amplitude of the variable force of the Kapitza pendulum, the Josephson frequency Ω_J corresponds to the oscillation frequency of the suspension point, and the averaged magnetic moment components specify a stable position. In our recent work [42] an analytical description of the magnetic moment reorientation features under ac voltage drive and manifestations of the Kapitza pendulum phenomenon was reported.

In the present paper, we investigate the resonance phenomena and develop a general analytical description of the resonance features which is applicable to several types of superconducting and magnetic hybrid heterostructures. The mechanical analogy for this system is two coupled oscillators with an external periodic force applied to one of them. We show that such a system has rich resonance physics.

The structure of the paper is as follows. In Sec. II, we introduce the model. The analytical description of the resonance properties of the system is provided in Sec. III. A comparison of analytical and numerical results, and a discussion of some special cases are presented in Sec. IV. The conclusions are presented in Sec. V.

II. MODEL AND METHODS

A voltage biased JJ of length l coupled to a nanomagnet of magnetic moment $\mathbf{M} = (M_x, M_y, M_z)$ is located at a distance $\mathbf{r}_M = a\mathbf{e}_x$ from the center of the junction, as shown in Fig. 1(a). The anisotropy energy of the nanomagnet is given by

$$E_M = \frac{-Kv}{2} \left(\frac{M_y}{M_0} \right)^2, \quad (1)$$

where K is the anisotropy constant, v is the volume of the nanomagnet, M_y is magnetization in the y direction (easy axis), and $M_0 = |\mathbf{M}|$ is the modulus of the magnetization

vector. The dc and ac voltages applied to the JJ generate the magnetic field acting on the nanomagnet. Therefore, the effective field is given by [38,39,41]

$$\mathbf{H}_{\text{eff}} = -\frac{dE}{d\mathbf{M}} = -\frac{dE_M}{d\mathbf{M}} + \frac{d}{d\mathbf{M}} I \int d\mathbf{r} \mathbf{A}(\mathbf{r}, \tau), \quad (2)$$

where E is the total energy of the system, and $\mathbf{A} = \frac{\mu_0}{4\pi} \frac{\mathbf{M} \times \mathbf{r}}{r^3}$ is the vector potential created at a distance r from the nanomagnet, which is assumed to be much smaller than all other dimensions of the problem. The last term is the magnetic field H_J created by the total current I through the Josephson junction [41].

The dynamics of the nanomagnet's magnetic moment can be described by the Landau-Lifshitz-Gilbert (LLG) equation

$$\frac{d\mathbf{M}}{d\tau} = \gamma \mathbf{H}_{\text{eff}} \times \mathbf{M} + \frac{\alpha}{M_0} \left(\mathbf{M} \times \frac{d\mathbf{M}}{d\tau} \right), \quad (3)$$

where α is the Gilbert damping parameter and γ is the gyromagnetic ratio. In dimensionless quantities the magnetic moment components in the LLG equation are given by

$$\frac{dm_x}{dt} = \frac{\Omega_F}{(1+\alpha^2)} [h_y(m_z - \alpha m_x m_y) - h_z(\alpha m_x m_z + m_y) + \alpha h_x(m_y^2 + m_z^2)], \quad (4a)$$

$$\frac{dm_y}{dt} = \frac{\Omega_F}{(1+\alpha^2)} [-h_x(\alpha m_x m_y + m_z) + h_z(m_x - \alpha m_y m_z) + \alpha h_y(m_x^2 + m_z^2)], \quad (4b)$$

$$\frac{dm_z}{dt} = \frac{\Omega_F}{(1+\alpha^2)D} [\alpha \tilde{h}_z(m_x^2 + m_y^2) - h_y(m_x + \alpha m_y m_z) + h_x(m_y - \alpha m_x m_z)], \quad (4c)$$

where $m_i = M_i/M_0$ ($i = x, y, z$) are the normalized components of the magnetic moment, h_i are the effective field components normalized to $H_F = \omega_F/\gamma$, $\Omega_F = \omega_F/\omega_c$ is the normalized frequency of the ferromagnetic resonance, $\omega_c = 2eRI_c/\hbar$ is the characteristic Josephson frequency, I_c is the critical current of the JJ, R is the resistance of the JJ, $t = \tau\omega_c$ is the normalized time, $D = 1 + \frac{\Omega_F \alpha \epsilon k}{1+\alpha^2} (m_x^2 + m_y^2)$, $\epsilon = Gk$, $G = \epsilon_J/Kv$ is the Josephson to magnetic energy ratio, $\epsilon_J = \Phi_0 I_c/2\pi$ is the Josephson energy, Φ_0 is the flux quantum, and $k = (1/2\Phi_0)\mu_0 v M_0 l/a\sqrt{l^2 + a^2}$ is the coupling constant between the JJ and the nanomagnet.

The components of the total effective field can be obtained by using the Biot-Savart law to calculate the magnetic field acting on the nanomagnet generated by the Josephson junction, so they are given by

$$h_x = 0,$$

$$h_y = m_y,$$

$$h_z = \tilde{h}_z - \epsilon k \dot{m}_z,$$

$$\tilde{h}_z = \epsilon \left[\sin \left(Vt - km_z + \frac{A}{\omega_R} \sin(\omega_R t) \right) + V + A \cos(\omega_R t) \right], \quad (5)$$

where V is the dc voltage bias normalized to $V_c = \hbar\omega_c/2e$, $A = V_{ac}/V_c$ is the amplitude of the external drive, and ω_R is the frequency of the external drive normalized to ω_c . Notice

also that in our normalization the dc voltage bias V is equal to the Josephson frequency ω_J .

III. ANALYTICAL DESCRIPTION

We consider that both DC and AC voltages are applied to the JJ, so the nanomagnet is subjected to two periodic drives. The first one is due to the oscillating magnetic field generated by Josephson oscillations of the DC voltage biased JJ. This magnetic field excites the precession of the magnetic moment of the nanomagnet and leads to a ferromagnetic resonance when the precession frequency equals the eigenfrequency ω_F of the magnetic system. The second drive, due to the ac voltage applied to the JJ, leads to the ‘‘Kittel’’ ferromagnetic resonance when the ac frequency equals the eigenfrequency ω_F of the magnetic system. For experimental realization of such a system, we estimate the model parameters according to Ref. [44], based on Refs. [45–48]. We consider a nanomagnet

with an anisotropy constant of 20 KJm^{-3} , saturation magnetization of 1950 KAm^{-1} , and volume $2 \times 10^{-22} \text{ m}^3$, while the Gilbert damping parameter is $\alpha \sim 0.0001 - 0.1$. On the other hand, for typical Josephson junctions the Josephson energy is $\epsilon_J \sim 1.97 \times 10^{-18} \text{ J}$, the critical current is $I_c \sim \text{mA}$, and the normal state resistance of the junction is $\sim \text{m}\Omega$. Thus, the voltage is of the order of μV , the Josephson frequency is of the order of GHz, and the ferromagnetic resonance frequency of the nanomagnets is of the order of $\sim \text{GHz}$ [49,50]. In this section, we present an analytical description of the combined effect of these two drives, which predicts rich resonance physics.

It is easier to work in spherical coordinates, defining the projections of the magnetic moment in terms of the polar and azimuthal angles, namely, $m_x = \sin \theta \cos \phi$, $m_y = \sin \theta \sin \phi$, $m_z = \cos \theta$, where $\theta \in [0, \pi]$ and $\phi \in [0, 2\pi]$. Then, Eqs. (4) and (5) are translated into time derivatives of the angles, according to Appendix A of Ref. [42]:

$$\dot{\theta} = -\frac{\sin \theta \Omega_F}{1 + \alpha^2 + \alpha \epsilon k \sin^2 \theta \Omega_F} [\alpha \tilde{h}_z - \sin \phi (\cos \phi + \alpha \cos \theta \sin \phi)], \quad (6a)$$

$$\dot{\phi} = \frac{\Omega_F}{1 + \alpha^2 + \alpha \epsilon k \sin^2 \theta \Omega_F} [\tilde{h}_z + (\sin^2 \theta \cos \phi \epsilon k \Omega_F - \sin \phi \cos \theta + \alpha \cos \phi) \sin \phi], \quad (6b)$$

$$\tilde{h}_z(t) = \epsilon \sin[Vt - k \cos \theta + \frac{A}{\omega_R} \sin(\omega_R t)] + \epsilon[V + A \cos(\omega_R t)]. \quad (6c)$$

We note that superconducting current in the JJ under the influence of dc and ac drives represents a frequency modulated signal, where the dc Josephson frequency $V \equiv \omega_J$ is modulated by the term $A \cos(\omega_R t)$. Thus, JJ in this case creates ac magnetic field with a modulated frequency. Such a modulated signal can be represented through a superposition of harmonic signals applied to the nanomagnet as follows:

$$\sin \left[Vt - km_z + \frac{A}{\omega_R} \sin(\omega_R t) \right] = \sum_{m=-\infty}^{\infty} \text{sign}^m(m) J_{|m|} \left(\frac{A}{\omega_R} \right) \sin[(V + m\omega_R)t - k \cos \theta], \quad (7a)$$

$$\cos \left[Vt - km_z + \frac{A}{\omega_R} \sin(\omega_R t) \right] = \sum_{m=-\infty}^{\infty} \text{sign}^m(m) J_{|m|} \left(\frac{A}{\omega_R} \right) \cos[(V + m\omega_R)t - k \cos \theta], \quad (7b)$$

Plugging Eq. (7) into Eq. (6) we obtain an expansion for $\dot{\theta}$ and $\dot{\phi}$:

$$\dot{\theta} = -C(\theta) \sin \theta [F_0(\theta, \phi) + F_1(\theta, t)], \quad (8a)$$

$$\dot{\phi} = C(\theta) [Q_0(\theta, \phi) + Q_1(\theta, t)], \quad (8b)$$

where

$$C(\theta) = \frac{\Omega_F}{1 + \alpha^2 + \alpha \epsilon k \sin^2 \theta \Omega_F}. \quad (8c)$$

$$F_0(\theta, \phi) = \alpha \epsilon V - \sin \phi (\cos \phi + \alpha \cos \theta \sin \phi), \quad (8d)$$

$$F_1(\theta, t) = \alpha \epsilon A \cos(\omega_R t) + \alpha \epsilon \sum_{m=-\infty}^{\infty} \text{sign}^m(m) J_{|m|} \left(\frac{A}{\omega_R} \right) \sin[(V + m\omega_R)t - k \cos \theta], \quad (8e)$$

$$Q_0(\theta, \phi) = \epsilon V + (\sin^2 \theta \cos \phi \epsilon k \Omega_F - \sin \phi \cos \theta + \alpha \cos \phi) \sin \phi, \quad (8f)$$

$$Q_1(\theta, t) = \epsilon A \cos(\omega_R t) + \epsilon \sum_{m=-\infty}^{\infty} \text{sign}^m(m) J_{|m|} \left(\frac{A}{\omega_R} \right) \sin[(V + m\omega_R)t - k \cos \theta]. \quad (8g)$$

Notice that the terms $F_0(\theta, \phi)$ and $Q_0(\theta, \phi)$ do not depend explicitly on time. Therefore, if $F_1(\theta, t) = Q_1(\theta, t) = 0$ and the magnetization of the nanomagnet reaches a position (θ_0, ϕ_0) where

$$F_0(\theta_0, \phi_0) = Q_0(\theta_0, \phi_0) = 0, \quad (9)$$

it remains in that position. We call (θ_0, ϕ_0) the stationary point or stationary position. From (9) we get

$$\phi_0 = \frac{\pi}{2}, \frac{3\pi}{2}, \quad \text{and} \quad \cos \theta_0 = \begin{cases} \epsilon V & \text{for } |\epsilon V| \leq 1, \\ \text{sign}(V) & \text{for } |\epsilon V| > 1. \end{cases} \quad (10)$$

Nevertheless, even in the absence of the terms $F_1(\theta, t)$ and $Q_1(\theta, t)$, the system may or may not advance toward the stationary point. If there is a vicinity of (θ_0, ϕ_0) in which

the system advances toward the stationary point, we say that (θ_0, ϕ_0) is a stable point (or stable position), whereas if there is no such vicinity, then (θ_0, ϕ_0) is an unstable stationary point. In Appendix A, we show that for the chosen parameters the point corresponding to $\phi_0 = \pi/2$ is stable, whereas the point corresponding to $\phi_0 = 3\pi/2$ is unstable. Therefore, from now on we shall discuss only the stable point $(\theta_0, \phi_0 = \pi/2)$.

If the amplitude of the external perturbation is small, the system oscillates around the stable point. Expanding $F_0(\theta, t)$ and $Q_0(\theta, t)$ in series around (θ_0, ϕ_0) , keeping only the linear terms, using (7), and denoting $\tilde{\theta} \equiv \theta - \theta_0$, $\tilde{\phi} \equiv \phi - \phi_0$, Eqs. (8a) and (8b) become

$$\begin{aligned} \dot{\tilde{\theta}} &\approx -C(\theta_0) \sin(\theta_0) \left\{ \alpha \sin(\theta_0) \tilde{\theta} + \tilde{\phi} + \alpha \epsilon A \cos(\omega_R t) + \alpha \epsilon \sum_{m=-\infty}^{\infty} \text{sign}^m(m) J_{|m|} \left(\frac{A}{\omega_R} \right) \sin[(V + m\omega_R)t - k \cos(\theta_0)] \right\}, \\ \dot{\tilde{\phi}} &\approx C(\theta_0) \left\{ \sin(\theta_0) \tilde{\theta} - [\alpha + k\epsilon \Omega_F \sin^2(\theta_0)] \tilde{\phi} + \epsilon A \cos(\omega_R t) + \epsilon \sum_{m=-\infty}^{\infty} \text{sign}^m(m) J_{|m|} \left(\frac{A}{\omega_R} \right) \sin[(V + m\omega_R)t - k \cos(\theta_0)] \right\}. \end{aligned} \quad (11)$$

We split the system of Eq. (11) into an infinite number of systems of equations by writing

$$\tilde{\theta} \equiv \tilde{\theta}_{\omega_R} + \sum_{m=-\infty}^{\infty} \tilde{\theta}_m \quad \text{and} \quad \tilde{\phi} \equiv \tilde{\phi}_{\omega_R} + \sum_{m=-\infty}^{\infty} \tilde{\phi}_m. \quad (12)$$

The solutions of the system (11) in linear regime are given by:

$$\begin{aligned} \tilde{\theta} &= -A_{\theta\Omega} \sin(\omega_R t + \phi_{\omega_R} + \delta_{\theta\omega_R}) \\ &\quad - \sum_{m=-\infty}^{\infty} A_{\theta m} \sin(\omega_m t + \phi_{\omega_R}), \\ \tilde{\phi} &= -A_{\phi\Omega} \sin(\omega_R t + \phi_{\omega_R} + \delta_{\phi\omega_R}) \\ &\quad - \sum_{m=-\infty}^{\infty} A_{\phi m} \sin(\omega_m t + \phi_{\omega_R} + \delta_{\phi m}), \end{aligned} \quad (13)$$

where $\omega_m \equiv V + m\omega_R$ and the amplitudes are

$$\begin{aligned} A_{\theta\Omega} &= \epsilon A \frac{\tilde{A}_{\theta} \left(\frac{\omega_R}{\Omega_F} \right)}{f \left(\frac{\omega_R}{\Omega_F} \right)}, \\ A_{\phi\Omega} &= \epsilon A \frac{\tilde{A}_{\phi} \left(\frac{\omega_R}{\Omega_F} \right)}{\sqrt{f \left(\frac{\omega_R}{\Omega_F} \right)}}, \end{aligned} \quad (14)$$

and

$$\begin{aligned} A_{\theta m} &= \epsilon \text{sign}^m(m) J_{|m|} \left(\frac{A}{\omega_R} \right) \frac{\tilde{A}_{\theta} \left(\frac{\omega_m}{\Omega_F} \right)}{f \left(\frac{\omega_m}{\Omega_F} \right)}, \\ A_{\phi m} &= \epsilon \text{sign}^m(m) J_{|m|} \left(\frac{A}{\omega_R} \right) \frac{\tilde{A}_{\phi} \left(\frac{\omega_m}{\Omega_F} \right)}{\sqrt{f \left(\frac{\omega_m}{\Omega_F} \right)}}. \end{aligned} \quad (15)$$

The functions \tilde{A}_{θ} , \tilde{A}_{ϕ} , and f are defined in Appendix B.

If we define $x \equiv \omega_R/\Omega_F$ [in (14)] or $x \equiv \omega_m/\Omega_F$ [in (15)], we observe that for the chosen parameters the ratios $\tilde{A}_{\theta}(x)/f(x)$ and $\tilde{A}_{\phi}(x)/f(x)$ have sharp maxima at $x_{\text{res}} \approx 1$,

which we will call resonances. These resonances are due to the fact that $f(x)$ has a minimum very close to zero, which corresponds (approximately) to x_{res} . So from the equation $df(x)/d(x^2) = 0$ we get

$$\begin{aligned} x_{\text{res}} &= \{2(1 - \alpha\epsilon k\Omega_F) \sin^2 \theta_0 - [\alpha^2 + (\epsilon k\Omega_F)^2] \\ &\quad \times \sin^4 \theta_0 - \alpha^2\} / \{2(1 + \alpha^2 + \alpha\epsilon k\Omega_F \sin^2 \theta_0)^2\}^{1/2} \\ &\approx 1 \quad \text{for} \quad \alpha, \epsilon k\Omega_F \ll 1. \end{aligned} \quad (16)$$

Therefore, resonances appear in the system at

$$\begin{aligned} \Omega_{\text{res}} &= x_{\text{res}} \Omega_F \approx \Omega_F \\ |\omega_{m,\text{res}}| &\equiv |V + m\Omega| = x_{\text{res}} \Omega_F \approx \Omega_F, \end{aligned} \quad (17)$$

respectively. If we denote

$$\begin{aligned} M_{\theta} &\equiv \frac{\tilde{A}_{\theta}(x_{\text{res}})}{f(x_{\text{res}})}, \\ M_{\phi} &\equiv \frac{\tilde{A}_{\phi}(x_{\text{res}})}{\sqrt{f(x_{\text{res}})}}, \end{aligned} \quad (18)$$

the expressions of the amplitudes at resonances (14) and (15) are simplified to

$$A_{\theta\Omega} = \epsilon A M_{\theta}, \quad A_{\phi\Omega} = \epsilon A M_{\phi}, \quad (19a)$$

and

$$\begin{aligned} A_{\theta m} &= \epsilon \text{sign}^m(m) J_{|m|} \left(\frac{A}{\omega_R} \right) M_{\theta}, \\ A_{\phi m} &= \epsilon \text{sign}^m(m) J_{|m|} \left(\frac{A}{\omega_R} \right) M_{\phi}, \end{aligned} \quad (19b)$$

respectively. We notice that the amplitude at resonance increases linearly with the amplitude of the external radiation in (19a) and varies with A as a Bessel function in (19b). We emphasize that the Bessel dependence appears because one of the periodical signals which is applied to the nanomagnet has a modulated frequency.

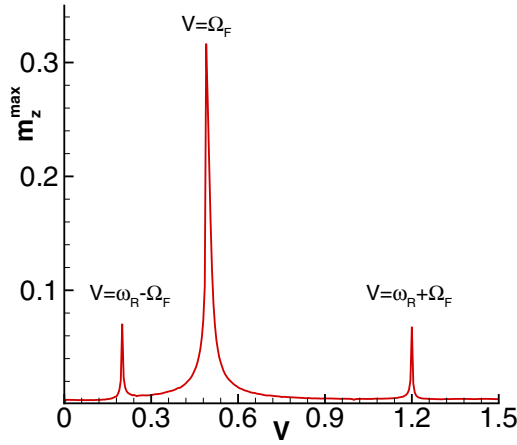


FIG. 2. Manifestation of the ferromagnetic resonance on the dependence $m_z^{\max}(V)$ at $\Omega_F = 0.5$, $\alpha = 0.001$, $G = 0.3$, $k = 0.01$, $A = 0.1$, and $\omega_R = 0.7$.

IV. DISCUSSION

Here we present the results of numerical simulations of the system of Eq. (4) and provide a thorough comparison with the obtained analytical expressions. Figure 2 shows the maximum amplitude of m_z oscillations as a function of V , for $\omega_R = 0.7$. A ferromagnetic resonance peak is observed at a voltage corresponding to the frequency of the Josephson oscillations $\omega_J = 0.5$. The results for m_x^{\max} and m_y^{\max} are qualitatively the same and are not presented. We note that in agreement with Eq. (17) for $m = \pm 1$, additional peaks are observed at frequencies $\omega_R - \Omega_F$ and $\omega_R + \Omega_F$.

The amplitudes of oscillations at $V = \Omega_F$ and $V = \omega_R - \Omega_F$ are plotted in Fig. 3 as functions of A . These choices of frequencies correspond approximately to the resonances $\omega_{0,\text{res}} = V_{\text{res}} = x_{\text{res}} \Omega_F \approx \Omega_F$ and $\omega_{-1,\text{res}} = (V - \omega_R)_{\text{res}} = x_{\text{res}} \Omega_F \approx \Omega_F$. We observe that the amplitudes approximately follow

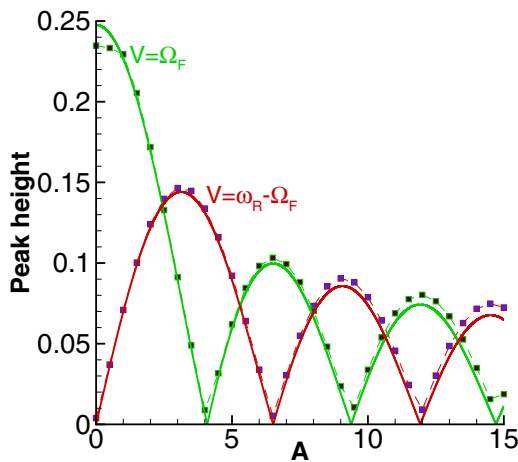


FIG. 3. The heights of the resonance peaks as a function of the amplitude A at $\Omega_F = 0.5$, $\alpha = 0.01$, $G = 0.01$, $k = 0.53$, and $\omega_R = 1.7$. Symbols are simulated from the system of Eq. (4), and solid lines are analytical approximations using (19b). The red lines are the height of the resonance peak $V \approx \omega_R - \Omega_F$. The green lines are the height of the resonance peak $V \approx \Omega_F$.

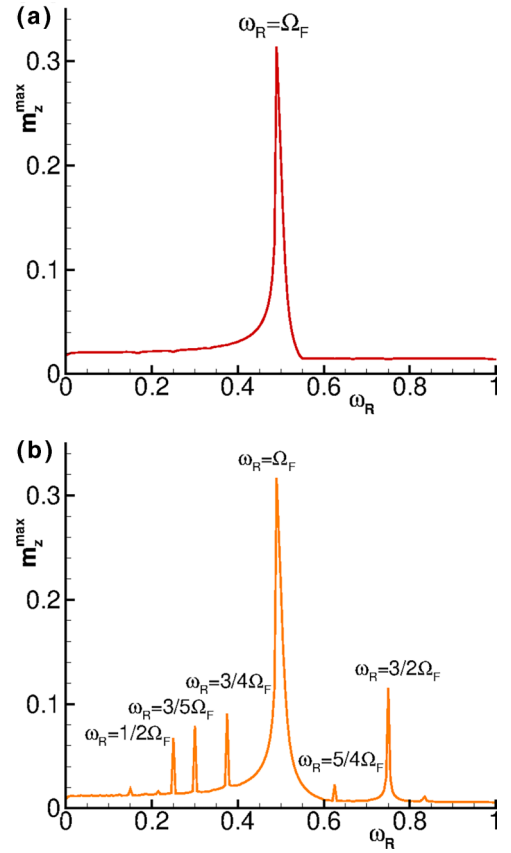


FIG. 4. Manifestation of the ferromagnetic resonance $\Omega_F = \omega_R \neq V$ on the dependence $m_z^{\max}(\omega_R)$ at $\Omega_F = 0.5$, $\alpha = 0.001$, $G = 0.3$, $k = 0.01$, $A = 1$ and (a) $V = 5$, (b) $V = 2$.

the Bessel function behavior of (19b). The symbols in Fig. 3 are simulated from the system of Eq. (4). Notice that the figure demonstrates an almost perfect matching between the analytically obtained and numerically simulated results. We note that the heights of the resonance peaks (as a function of A) oscillate differently, depending on the order of the Bessel function. For example, while the height of the peak corresponding to $V \approx \Omega_F$ is proportional to $J_0(\frac{A}{\omega_R})$, the height of the peak corresponding to $\omega_{-1,\text{res}} = (V - \omega_R)_{\text{res}} \approx \Omega_F$ is proportional to $J_1(\frac{A}{\omega_R})$. Therefore, the position of resonances can be determined by (17) and their heights are determined by (19b). This feature allows one to change the position and the intensity of different resonances by the amplitude and the frequency of the external periodic drive. The first resonance condition in (17) can be realized with a variation of ω_R at fixed value of V .

Figure 4 shows the calculated maximum amplitude of oscillations m_z^{\max} as a function of the periodic drive frequency ω_R at different values of V . A ferromagnetic resonance peak is observed [see Fig. 4(a)] at the frequency corresponding to $\omega_R \approx \Omega_F$ that is formed by $A_{\theta\omega_R}$ (19a). In Fig. 4(b) we reduced the value of V and additional peaks appeared in the frequency interval $\omega_R \in (0, 1)$ corresponding to the resonances of the amplitudes $A_{\theta m}$ (19b) at different values of m : $(-6, -10, -5, -4, -2)$ (from left to right) when the value of V is reduced ($V = 2$). They appear because distance in frequency between the peaks reduces according to (17).

So, the smaller the difference between Ω and corresponding Josephson frequency ($V \equiv \omega_j$), the smaller the distance between the resonance peaks. In Fig. 4(a) the corresponding peaks do not appear within the presented region. Note that these resonances, strongly dependent on the driving amplitudes, are similar to Kittel's ferromagnetic resonance.

The obtained results can be used to calculate the resonance condition for the ϕ_0 Josephson junction, where the phase shift φ_0 in the current-phase relation is proportional to the magnetic moment perpendicular to the gradient of the asymmetric spin-orbit potential [51,52] [43], by neglecting the effective field due to quasiparticle current [the term $V + A \cos(\omega_R t)$ in (5)]. In this case, we immediately obtain

$$A_{\theta\omega_R} = A_{\phi\omega_R} = 0 \quad (20)$$

and

$$A_{\theta m} = \epsilon \operatorname{sign}^m(m) J_{|m|}(A/\omega_R) \frac{\sqrt{1+3\alpha^2}}{2\alpha}, \quad (21a)$$

$$A_{\phi m} = \epsilon \operatorname{sign}^m(m) J_{|m|}(A/\omega_R) \frac{\sqrt{1-\alpha^2}}{2\alpha}. \quad (21b)$$

Furthermore, the results presented in Ref. [41] can be obtained at $A = 0$. In this case, only the term $m = 0$ ($\omega_{m=0} = V$) survives and Eq. (19) becomes

$$A_{\theta m} = \epsilon \frac{\tilde{A}_\theta\left(\frac{V}{\Omega_F}\right)}{f\left(\frac{V}{\Omega_F}\right)} \quad (22a)$$

and

$$A_{\phi m} = \epsilon \frac{\tilde{A}_\phi\left(\frac{V}{\Omega_F}\right)}{\sqrt{f\left(\frac{V}{\Omega_F}\right)}}. \quad (22b)$$

The resonances can now be observed as maxima of $A_{\theta m}$ and $A_{\phi m}$ as functions of V and formulas (17) transform to $V_{\text{res}} \equiv x_{\text{res}} \Omega_F$.

Therefore, the derived analytical description presented in Sec. III is universal and could be applied to various systems such as superconducting and magnetic heterostructures (ϕ_0 Josephson junction, nanomagnet coupled to the JJ), and non-linear pendulum.

V. CONCLUSIONS

We present a thorough analytical description and classification of possible resonances arising in the system. The amplitudes of the induced oscillations $A_{\theta\Omega}(V, \omega_R, \Omega_F)$ and $A_{\theta m}(\omega_m, \omega_R, \Omega_F)$ are calculated in the linear approximation. They have very sharp maxima (resonances) at Ω_{res} and $\omega_{m,\text{res}}$, respectively, which can be found numerically, in general. When $\alpha, \epsilon \ll 1$, both Ω_{res} and $\omega_{m,\text{res}}$ are approximately equal to Ω_F . In the limit $\alpha, \epsilon \rightarrow 0$, we have $\Omega_{\text{res}}, \omega_{m,\text{res}} \rightarrow \Omega_F$ and the amplitudes $A_{\theta\omega_R}, A_{\theta m}$ diverge.

We demonstrated resonance effects in a system consisting of the nanomagnet coupled to the Josephson junction under

the influence of the external periodic drive of frequency ω_R . It has been shown that the magnetic dynamics of such a system manifests additional resonances at $V + m\omega_R \approx \Omega_F$, where m is an integer. We found that the heights of the resonance peaks strongly depend on the amplitude of the external periodic drive. Therefore, by changing the amplitude, it is possible to suppress the main ferromagnetic resonance ($V = \Omega_F$) and enhance resonances at $V = |\Omega_F + m\omega_R|$. This represents a method for controlling the resonance properties of the system by adjusting the driving frequency and amplitude. In other words, by applying an external periodic drive, one can generate specific resonances at voltages $V \approx \Omega_F + m\omega_R$ and, at the same time, suppress the FMR at $V = \Omega_F$. This method provides wide opportunities for experimental applications.

Our results are of practical importance. It is known, that one of the methods for determining the characteristics of magnetic systems is FMR. The standard FMR theory based on microwave absorption in magnetic materials shows that the resonant frequency is the functions of the effective field, material, and system parameters. These dependences can be used to determine the parameters of the material. On the other hand, these parameters can be varied to control the microwave absorption properties of the material. This two-way relationship between the FMR characteristics and the physical parameters of the system is usually based on analytical expressions that give the resonant frequency as a function of the material parameters (anisotropy constants, exchange and dipole couplings, etc.). In the case of hybrid structures, however, such analytical expressions cannot be obtained and one has to resort to numerical simulation or some approximate solution. Our analytical results provide necessary information to estimate the ferromagnetic resonance frequency [using (17)] and damping parameter [using (19) and (B5) from the Appendix] in hybrid structures of the SFS and JJ-NM types, and can have applications related to the resonance properties of hybrid structures as well as in quantum information processing and spintronics.

ACKNOWLEDGMENTS

The reported study was funded by the (ASRT, Egypt)-(JINR, Russia) research projects. Numerical simulations were funded by Project No. 22-71-10022 of the Russian Scientific Fund. D.V.A. and M.D. acknowledge the financial support from UEFISCDI (Romania), projects PN 23210101/2023 and PN 23210204/2023. Special thanks are due to the BLTP, HybriLIT heterogeneous computing platform (LIT, JINR Russia) and Bibliotheca Alexandrina (Egypt) for the HPC servers.

APPENDIX A: THE STATIONARY POINT

To determine the stability of the stationary points (10), we calculate the projection of the velocity $\mathbf{v} \equiv (\dot{\theta}, \dot{\phi})$ on the unit vector $\hat{\mathbf{s}} \equiv [(\theta_0 - \theta)/u, (\phi_0 - \phi)/u]$, which gives the direction from the current point (θ, ϕ) to the stationary point (θ_0, ϕ_0) (where $u = \sqrt{(\theta_0 - \theta)^2 + (\phi_0 - \phi)^2}$):

$$P(\theta, \phi) \equiv \mathbf{v} \cdot \hat{\mathbf{s}} = \frac{1}{\sqrt{(\theta_0 - \theta)^2 + (\phi_0 - \phi)^2}} \{(\theta_0 - \theta) \sin \theta [\alpha \epsilon V - \sin \phi (\cos \phi + \alpha \cos \theta \sin \phi)] + (\phi_0 - \phi)\}$$

$$\times [\epsilon V + (\epsilon k \Omega_F \sin^2 \theta \cos \phi - \sin \phi \cos \theta + \alpha \cos \phi) \sin \phi]. \quad (\text{A1})$$

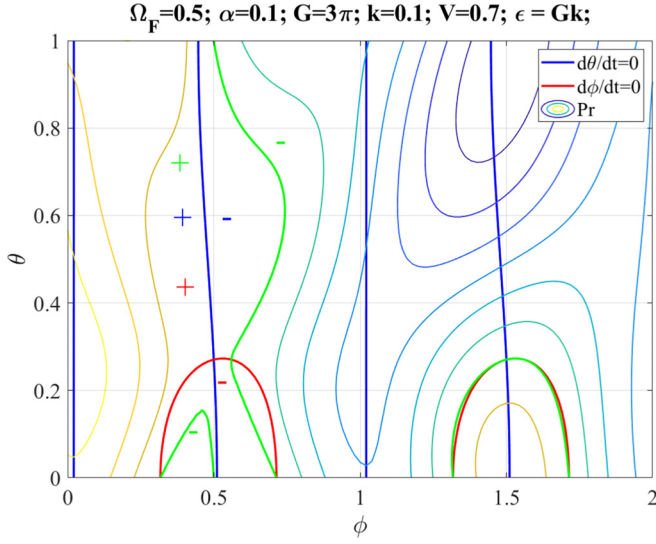


FIG. 5. The contours corresponding to $F_0(\theta, \phi) = 0$ (blue thick solid line), $Q_0(\theta, \phi) = 0$ (red thick solid lines), and $P(\theta, \phi) = 0$ (green thick solid lines). By the colored signs + and - we indicate the signs of the corresponding functions: blue + and - signs indicate the regions in which $F_0(\theta, \phi) > 0$ and $F_0(\theta, \phi) < 0$, respectively, bordered by the thick blue solid line; red + and - signs indicate the regions in which $Q_0(\theta, \phi) > 0$ and $Q_0(\theta, \phi) < 0$, respectively, bordered by the thick red solid line; green + and - signs indicate the regions in which $P(\theta, \phi) > 0$ and $P(\theta, \phi) < 0$, respectively, bordered by the thick green solid line.

In the absence of external time dependent perturbations [i.e., $F_1(\theta, t) = 0$ and $Q_1(\theta, t) = 0$], if $P(\theta, \phi) > 0$, the magnet moves toward the stationary point, whereas the magnet moves away from the stationary point if $P(\theta, \phi) < 0$. In Fig. 5 we see two stationary points (the intersections of the red and blue solid lines) and observe that, for the chosen parameters, the point corresponding to $(\phi_0 = \pi/2)$ is in the region $P(\theta, \phi) > 0$, whereas the point $(\phi_0 = 3\pi/2)$ is in the region $P(\theta, \phi) < 0$.

APPENDIX B: THE ELEMENTARY OSCILLATIONS

In system (11), we redefine $\tilde{\theta}$ and $\tilde{\phi}$ according to (12). The new variables describe “individual” oscillations of specified frequencies: the variables $(\tilde{\theta}_{\omega_R}, \tilde{\phi}_{\omega_R})$ for the frequency ω_R and the variables $(\tilde{\theta}_m, \tilde{\phi}_m)$ for the frequencies $\omega_m \equiv V + m\omega_R$. These oscillations satisfy the systems of equations

$$\begin{aligned} \dot{\tilde{\theta}}_{\omega_R} &= -C(\theta_0) \sin(\theta_0) \{ \alpha \sin(\theta_0) \tilde{\theta}_{\omega_R} \\ &\quad + \tilde{\phi}_{\omega_R} + \alpha \epsilon A \cos(\omega_R t) \}, \\ \dot{\tilde{\phi}}_{\omega_R} &= C(\theta_0) \{ \sin(\theta_0) \tilde{\theta}_{\omega_R} - [\alpha + k \epsilon \Omega_F \sin^2(\theta_0)] \tilde{\phi}_{\omega_R} \\ &\quad + \epsilon A \cos(\omega_R t) \}, \end{aligned} \quad (\text{B1})$$

and

$$\begin{aligned} \dot{\tilde{\theta}}_m &= -C(\theta_0) \sin(\theta_0) \left\{ \alpha \sin(\theta_0) \tilde{\theta}_m + \tilde{\phi}_m + \alpha \epsilon \text{sign}^m(m) J_{|m|} \left(\frac{A}{\omega_R} \right) \sin[\omega_m t - k \cos(\theta_0)] \right\}, \\ \dot{\tilde{\phi}}_m &= C(\theta_0) \left\{ \sin(\theta_0) \tilde{\theta}_m - [\alpha + k \epsilon \Omega_F \sin^2(\theta_0)] \tilde{\phi}_m + \epsilon \text{sign}^m(m) J_{|m|} \left(\frac{A}{\omega_R} \right) \sin[\omega_m t - k \cos(\theta_0)] \right\}, \end{aligned} \quad (\text{B2})$$

where $m \in \mathbb{Z}$ (integer). By this decomposition we show that the movement of the nanomagnet (11) is a superposition of an infinite number of oscillations of frequencies ω_R , and $\omega_m \equiv V + m\omega_R$. The system (B1) has solutions of the form

$$\begin{aligned} \tilde{\theta}_{\omega_R} &= \frac{C_2(\eta + \sqrt{\chi} + 2P)}{2 \sin \theta_0} e^{\frac{(\eta + \sqrt{\chi})C(\theta) t}{2}} + \frac{C_1(\eta - \sqrt{\chi} + 2P)}{2 \sin \theta_0} e^{\frac{(\eta - \sqrt{\chi})C(\theta) t}{2}} - A_{\theta \omega_R} \sin(\omega_R t + \phi_{\omega_R} + \delta_{\theta \omega_R}), \\ \tilde{\phi}_{\omega_R} &= C_2 e^{\frac{(\eta + \sqrt{\chi})C(\theta) t}{2}} + C_1 e^{\frac{(\eta - \sqrt{\chi})C(\theta) t}{2}} - A_{\phi \omega_R} \sin(\omega_R t + \phi_{\omega_R} + \delta_{\phi \omega_R}), \end{aligned} \quad (\text{B3})$$

whereas the solutions of the system (B2) are

$$\begin{aligned} \tilde{\theta}_m &= \frac{C_2(\eta + \sqrt{\chi} + 2P)}{2 \sin \theta_0} e^{\frac{(\eta + \sqrt{\chi})C(\theta) t}{2}} + \frac{C_1(\eta - \sqrt{\chi} + 2P)}{2 \sin \theta_0} e^{\frac{(\eta - \sqrt{\chi})C(\theta) t}{2}} - A_{\theta m} \sin(\omega_m t + \phi_{\omega_R}), \\ \tilde{\phi}_m &= C_2 e^{\frac{(\eta + \sqrt{\chi})C(\theta) t}{2}} + C_1 e^{\frac{(\eta - \sqrt{\chi})C(\theta) t}{2}} - A_{\phi m} \sin(\omega_m t + \phi_{\omega_R} + \delta_{\phi m}), \end{aligned} \quad (\text{B4})$$

where $P \equiv \alpha + k \epsilon \Omega_F \sin^2 \theta_0$, $\chi \equiv (\alpha \sin^2 \theta_0 - P)^2 - 4 \sin^2 \theta_0$, $\eta \equiv -(\alpha \sin^2 \theta_0 + P)$, and $\xi_0 \equiv C(\theta_0)^2 (P\alpha + 1) \sin^2 \theta_0$ (by ϕ_{ω_R} we denote an arbitrary phase).

Since $(\eta \pm \sqrt{\chi}) < 0$, the terms proportional to C_1 and C_2 decay in time and only the oscillatory terms remain. Therefore, in the linear regime the solutions (B3) and (B4) could be combined and substituted into (12) to obtain Eq. (13) with the amplitudes (14) and (15).

In Eqs. (14) and (15) we have the notation

$$f(x) = \frac{\Gamma_1^2 x^4 + [(\alpha^2 + \Gamma_2^2) \sin^4 \theta_0 + 2(\alpha \Gamma_2 - 1) \sin^2 \theta_0 + \Gamma_2^2] x^2 + \sin^4 \theta_0}{\Gamma_1^2}, \quad (\text{B5a})$$

$$\tilde{A}_\theta(x) = \frac{\sin \theta_0}{\Gamma_1} \left\{ \frac{[\sin^2 \theta_0 + (\alpha^2 \sin^2 \theta_0 - 1)x^2]^2}{\Gamma_1^2} + \left(\frac{\alpha + \Gamma_2 \sin^2 \theta_0}{\Gamma_1} + \alpha x^2 \right)^2 x^2 \right\}^{1/2}, \quad (\text{B5b})$$

$$\tilde{A}_\phi(x) = \frac{1}{(1 + \alpha^2 + \Gamma_2 \sin^2 \theta_0)} x, \quad (\text{B5c})$$

where $\Gamma_1 = 1 + \alpha^2 + \alpha \epsilon k \Omega_F \sin^2 \theta_0$, $\Gamma_2 = \epsilon k \Omega_F$.

In the notation (B5), we consider f , \tilde{A}_θ , and \tilde{A}_ϕ as functions of x . The phases of Eqs. (B3) and (B4) are defined by the relations

$$\begin{aligned} \sin \delta_{\theta\omega_R} &= \frac{\xi_0 \left[\xi_0 + \frac{\omega_R^2 (\alpha^2 \sin^2 \theta_0 - 1)}{\alpha P + 1} \right]}{\sqrt{\xi_0^2 \left[\xi_0 + \frac{\omega_R^2 (\alpha^2 \sin^2 \theta_0 - 1)}{\alpha P + 1} \right]^2 + C(\theta_0)^2 \omega_R^2 (P \xi_0 + \omega_R^2 \alpha \sin^2 \theta_0)^2}}, \\ \cos \delta_{\theta\omega_R} &= \frac{C(\theta_0) \omega_R (P \xi_0 + \omega_R^2 \alpha \sin^2 \theta_0)}{\sqrt{\xi_0^2 \left[\xi_0 + \frac{\omega_R^2 (\alpha^2 \sin^2 \theta_0 - 1)}{\alpha P + 1} \right]^2 + C(\theta_0)^2 \omega_R^2 (P \xi_0 + \omega_R^2 \alpha \sin^2 \theta_0)^2}}, \\ \sin \delta_{\phi\omega_R} &= \frac{\omega_R C(\theta_0) \eta}{\sqrt{(\omega_R^2 - \xi_0)^2 + C(\theta_0)^2 \eta^2 \omega_R^2}}, \quad \cos \delta_{\phi\omega_R} = -\frac{(\omega_R^2 - \xi_0)}{\sqrt{(\omega_R^2 - \xi_0)^2 + C(\theta_0)^2 \eta^2 \omega_R^2}}, \\ \sin \delta_{\theta m} &= \frac{-C(\theta_0) \omega_R (P \xi_0 + \omega_R^2 \alpha \sin^2 \theta_0)}{\sqrt{\xi_0^2 \left[\xi_0 + \frac{\omega_R^2 (\alpha^2 \sin^2 \theta_0 - 1)}{P \alpha + 1} \right]^2 + C(\theta_0)^2 \omega_R^2 (P \xi_0 + \omega_R^2 \alpha \sin^2 \theta_0)^2}}, \\ \cos \delta_{\theta m} &= \frac{\xi_0 \left[\xi_0 + \frac{\omega_R^2 (\alpha^2 \sin^2 \theta_0 - 1)}{P \alpha + 1} \right]}{\sqrt{\xi_0^2 \left[\xi_0 + \frac{\omega_R^2 (\alpha^2 \sin^2 \theta_0 - 1)}{P \alpha + 1} \right]^2 + C(\theta_0)^2 \omega_R^2 (P \xi_0 + \omega_R^2 \alpha \sin^2 \theta_0)^2}}, \\ \sin \delta_{\phi m} &= \frac{\omega_R^2 - \xi_0}{\sqrt{(\omega_R^2 - \xi_0)^2 + C(\theta_0)^2 \eta^2 \omega_R^2}}, \quad \cos \delta_{\phi m} = \frac{\omega_R C(\theta_0) \eta}{\sqrt{(\omega_R^2 - \xi_0)^2 + C(\theta_0)^2 \eta^2 \omega_R^2}}. \end{aligned}$$

-
- [1] C. Stamm *et al.*, Two-dimensional magnetic particles, *Science* **282**, 449 (1998).
- [2] A. J. Almeida, A. Sahu, D. J. Norris, G. N. Kakazei, H. Kannan, M. S. Brandt *et al.*, Anisotropic magnetic resonance in random nanocrystal quantum dot ensembles, *ACS Omega* **5**, 11333 (2020).
- [3] T. R. Harvey, N. Rubiano da Silva, J. H. Gaida, M. Möller, A. Feist, S. Schäfer, and C. Ropers, Ultrafast electron microscopy for probing magnetic dynamics, *MRS Bull.* **46**, 711 (2021).
- [4] D. Makarov, O. M. Volkov, A. Kákay, O. V. Pylypovskiy, B. Budinská, and O. V. Dobrovolskiy, New dimension in magnetism and superconductivity: 3D and curvilinear nanoarchitectures, *Adv. Mater.* **34**, 2101758 (2022).
- [5] D. Kumar, T. Jin, R. Sbiaa, M. Kläui, S. Bedanta, S. Fukami *et al.*, Domain wall memory: Physics, materials, and devices, *Phys. Rep.* **958**, 1 (2022).
- [6] A. Pierrot *et al.*, Switching field distribution of ultradense arrays of single-crystalline magnetic nanowires, *Appl. Phys. Lett.* **122**, 262403 (2023).
- [7] C. Swoboda, M. Michael, and M. Guido, Control of spin-wave excitations in deterministic fractals, *Phys. Rev. B* **91**, 064416 (2015).
- [8] T. S. Shaposhnikova and R. F. Mamin, Electric polarization in small magnetic particles, *J. Surf. Investig.* **15**, 1282 (2021).
- [9] S. Jeong and L. Jaejin, Iterative signal detection scheme using multilayer perceptron for a bit-patterned media recording system, *Appl. Sci.* **10**, 8819 (2020).
- [10] W. Wu *et al.*, Large area high density quantized magnetic disks fabricated using nanoimprint lithography, *J. Vac. Sci. Technol. B* **16**, 3825 (1998).
- [11] G. A. Prinz, Magnetoelectronics, *Science* **282**, 1660 (1998).
- [12] A. Ardavan, O. Rival, J. J. L. Morton, S. J. Blundell, A. M. Tyryshkin, G. A. Timco, and R. E. P. Winpenny, Will spin-relaxation times in molecular magnets permit quantum information processing? *Phys. Rev. Lett.* **98**, 057201 (2007).
- [13] M. N. Leuenberger and D. Loss, Quantum computing in molecular magnets, *Nature (London)* **410**, 789 (2001).
- [14] A. R. Rocha, V. M. García-Suárez, S. W. Bailey, C. J. Lambert, J. Ferrer, and S. Sanvito, Towards molecular spintronics, *Nat. Mater.* **4**, 335 (2005).
- [15] L. Bogani and W. Wernsdorfer, Molecular spintronics using single-molecule magnets, *Nat. Mater.* **7**, 179 (2008).
- [16] S. Hikino, M. Mori, S. Takahashi, and S. Maekawa, Microwave-induced supercurrent in a ferromagnetic Josephson junction, *Supercond. Sci. Technol.* **24**, 024008 (2011).
- [17] B. Hillebrands and K. Ounadjela, *Spin Dynamics in Confined Magnetic Structures II* (Springer Berlin, Heidelberg, 2003).
- [18] L. Landau and E. Lifshitz, On the theory of the dispersion of magnetic permeability in ferromagnetic bodies, *Phys. Z. Sowjet.* **8**, 153 (1935).
- [19] M. Sharma, S. Pathak, and M. Sharm, *FMR Measurements of Magnetic Nanostructures*, in *Ferromagnetic resonance - theory and applications*, edited by O. Yalcin (InTech, July 2013) Chap. 4, pp. 93-110.

- [20] J. H. E. Griffiths, Anomalous high-frequency resistance of ferromagnetic metals, *Nature (London)* **158**, 670 (1946).
- [21] M. G. Inghram, R. J. Hayden, and D. C. Hess, Jr., Neutron induced activities in Lutecium, Ytterbium, and Dysprosium, *Phys. Rev.* **71**, 270 (1947); C. Kittel, On the gyromagnetic ratio and spectroscopic splitting factor of ferromagnetic substances, *Phys. Rev.* **76**, 743 (1949).
- [22] F. J. Owens, Ferromagnetic resonance observation of a phase transition in magnetic field-aligned Fe_2O_3 nanoparticles, *J. Magn. Magn. Mater.* **321**, 2386 (2009).
- [23] K. Miyake, S. M. Noh, T. Kaneko, H. Imamura, and M. Sashiki, Study on high-Frequency 3D magnetization precession modes of circular magnetic nano-Dots using coplanar wave guide vector network analyzer ferromagnetic resonance, *IEEE Trans. Magn.* **48**, 1782 (2012).
- [24] K. Zakeri, T. Kebe, J. Lindner, and M. Farle, Magnetic anisotropy of Fe/GaAs(0 0 1) ultrathin films investigated by in situ ferromagnetic resonance, *J. Magn. Magn. Mater.* **299**, L1 (2006).
- [25] A. Layadi, Theoretical study of resonance modes of coupled thin films in the rigid layer model, *Phys. Rev. B* **69**, 144431 (2004).
- [26] B. Liu, Y. Yang, D. Tang, B. Zhang, M. Lu, and H. Lu, The contributions of intrinsic damping and two magnon scattering on the ferromagnetic resonance linewidth in $[Fe_{65}Co_{35}/SiO_2]_n$ multilayer films, *J. Alloys Compd.* **524**, 69 (2012).
- [27] S. Schäfer, N. Pachauri, C. K. A. Mewes, T. Mewes, C. Kaiser, Q. Leng, and M. Pakala, frequency-selective control of ferromagnetic resonance linewidth in magnetic multilayers, *J. Appl. Phys.* **100**, 032402 (2012).
- [28] R. B. Parvatheeswara, O. Caltun, I. Dumitru, and L. Spinu, Ferromagnetic resonance parameters of ball-milled Ni-Zn ferrite nanoparticles, *J. Magn. Magn. Mater.* **304**, e752 (2006).
- [29] X. Wang, L. J. Deng, J. L. Xie, and D. Li, Observations of ferromagnetic resonance modes on FeCo-based nanocrystalline alloys, *J. Magn. Magn. Mater.* **323**, 635 (2011).
- [30] R. Patel and F. J. Owens, Ferromagnetic resonance and magnetic force microscopy evidence for above room temperature ferromagnetism in Mn doped Si made by a solid state sintering process, *Solid State Commun.* **152**, 603 (2012).
- [31] E. De Biasi Jr., E. Lima, C. A. Ramos, A. Butera, and R. D. Zysler, Effect of thermal fluctuations in FMR experiments in uniaxial magnetic nanoparticles: Blocked vs. superparamagnetic regimes, *J. Magn. Magn. Mater.* **326**, 138 (2013).
- [32] S. E. Barnes, M. Aprili, I. Petković, and S. Maekawa, Ferromagnetic resonance with a magnetic Josephson junction, *Supercond. Sci. Technol.* **24**, 024020 (2011).
- [33] M. Nashaat, A. E. Botha, and Y. M. Shukrinov, Devil's staircases in the IV characteristics of superconductor/ferromagnet/superconductor Josephson junctions, *Phys. Rev. B* **97**, 224514 (2018).
- [34] M. Nashaat and Y. M. Shukrinov, Ferromagnetic resonance and effect of supercurrent on the magnetization dynamics in S/F/S junctions under circularly polarized magnetic field, *Phys. Part. Nucl. Lett.* **17**, 79 (2020).
- [35] Yu. M. Shukrinov, I. R. Rahmonov, A. Janalizadeh, and M. R. Kollahchi, Anomalous Gilbert damping and Duffing features of the superconductor-ferromagnet-superconductor φ_0 Josephson junction, *Phys. Rev. B* **104**, 224511 (2021).
- [36] M. A. Silaev, Anderson-Higgs mass of magnons in superconductor/ferromagnet/superconductor systems, *Phys. Rev. Appl.* **18**, L061004 (2022).
- [37] I. A. Golovchanskiy, N. N. Abramov, O. V. Emelyanova, I. V. Shchetinin, V. V. Ryazanov, A. A. Golubov, and V. S. Stolyarov, Magnetization dynamics in proximity-coupled superconductor-ferromagnet-superconductor multilayers. II. Thickness dependence of the superconducting torque, *Phys. Rev. Appl.* **19**, 034025 (2023).
- [38] L. Cai and E. M. Chudnovsky, Interaction of a nanomagnet with a weak superconducting link, *Phys. Rev. B* **82**, 104429 (2010).
- [39] R. Ghosh, M. Maiti, Y. M. Shukrinov, and K. Sengupta, Magnetization-induced dynamics of a Josephson junction coupled to a nanomagnet, *Phys. Rev. B* **96**, 174517 (2017).
- [40] E. M. Lifshitz and L. P. Pitaevskii, *Course of Theoretical Physics, Theory of the Condensed State*, Vol. 9 (Butterworth Heinemann, Oxford, 1991); B. Hillebrands, and K. Ounadjela, *Spin Dynamics of Confined Magnetic Structures II* (Springer-Verlag, Berlin, 2003), pp. 1–26.
- [41] Yu. M. Shukrinov, M. Nashaat, I. R. Rahmonov, and K. V. Kulikov, Ferromagnetic resonance and the dynamics of the magnetic moment in a “Josephson junction-nanomagnet” system, *JETP Lett.* **110**, 160 (2019).
- [42] K. V. Kulikov, D. V. Anghel, A. T. Preda, M. Nashaat, M. Sameh, and Y. M. Shukrinov, Kapitza pendulum effects in a Josephson junction coupled to a nanomagnet under external periodic drive, *Phys. Rev. B* **105**, 094421 (2022).
- [43] Y. M. Shukrinov, A. Mazanik, I. R. Rahmonov, A. E. Botha, and A. Buzdin, Re-orientation of the easy axis in φ_0 -junction, *Europhys. Lett.* **122**, 37001 (2018).
- [44] M. Nashaat, M. Sameh, A. E. Botha, K. V. Kulikov, and Y. M. Shukrinov, Bifurcation structure and chaos in nanomagnet coupled to Josephson junction, *Chaos* **32**, 093142 (2022).
- [45] P. Mangin and R. Kahn, *Superconductivity: An Introduction* (Springer Int., Grenoble Sciences, Cham, Grenoble, 2017).
- [46] R. P. Cowburn, A. O. Adeyeye, and M. E. Welland, Controlling magnetic ordering in coupled nanomagnet arrays, *New J. Phys.* **1**, 16 (1999).
- [47] L. F. Yin, D. H. Wei, N. Lei, L. H. Zhou, C. S. Tian, G. S. Dong, X. F. Jin, L. P. Guo, Q. J. Jia, and R. Q. Wu, Magnetocrystalline anisotropy in permalloy revisited, *Phys. Rev. Lett.* **97**, 067203 (2006).
- [48] K. H. J. Buschow, *Concise Encyclopedia of Magnetic and Superconducting Materials* (Elsevier Science, Amsterdam, Netherlands, 2005).
- [49] Nekrashevich and D. Litvinov, Ferromagnetic resonance in coupled magnetic nanostructured arrays, *AIP Adv.* **8**, 085002 (2018).
- [50] J. L. Déjardin, A. Franco, F. Vernay, and H. Kachkachi, Ferromagnetic resonance of a two-dimensional array of nanomagnets: Effects of surface anisotropy and dipolar interactions, *Phys. Rev. B* **97**, 224407 (2018).
- [51] A. Buzdin, Direct coupling between magnetism and superconducting current in the Josephson φ_0 junction, *Phys. Rev. Lett.* **101**, 107005 (2008).
- [52] F. Korschelle and A. Buzdin, Magnetic moment manipulation by a Josephson current, *Phys. Rev. Lett.* **102**, 017001 (2009).